# **RESEARCH PAPER**

# Application of Calcium Phosphate Nanoparticles Incorporated on Chitosan-Carbon Nanotubes (CaP@CS-CNT) for Investigation of Physiochemical and Mechanical of Bone Cement

Gulnoz Rakhimova <sup>1</sup>\*, Azizkhon Khashimov <sup>2</sup>, Baxtiyor Aripov <sup>3</sup>, Tokhir Aglamov <sup>4</sup>, Chori Bobokulov <sup>5</sup>, Kamola Yakhyaeva <sup>6</sup>, Khurshed Kurbonov <sup>7</sup>, Islom Kadirov <sup>8</sup>, Isroil Mo'minov <sup>9</sup>, Ikrom Abdullayev <sup>1</sup>, Shamshod Axmedov <sup>1</sup>, Bunyod Kendjaev <sup>10</sup>, Nafosat Ibrokhimova <sup>11</sup>

- <sup>1</sup> Bukhara State Medical Institute named after Abu Ali ibn Sino, Bukhara, Uzbekistan
- <sup>2</sup> Fergana Medical Institute of Public Health, Fergana, Uzbekistan
- <sup>3</sup> Bukhara State University, Bukhara, Uzbekistan
- <sup>4</sup> Bukhara State Pedagogical Institute, Bukhara, Uzbekistan
- <sup>5</sup> Termez University of Economics and Service, Termez, Uzbekistan
- <sup>6</sup> Tashkent State Medical University, Tashkent, Uzbekistan
- <sup>7</sup> Samarkand State Medical University, Samarkand, Uzbekistan
- <sup>8</sup> Urgench State University named after Abu Raykhan Beruni, Urgench, Uzbekistan
- <sup>9</sup> Termez State Pedagogical Institute, Termez, Uzbekistan
- <sup>10</sup> Urganch Innovation University, Urgench, Uzbekistan
- <sup>11</sup> Samarkand State University named after Sharof Rashidov, Uzbekistan

#### ARTICLE INFO

## Article History:

Received 15 June 2025 Accepted 17 September 2025 Published 01 October 2025

# Keywords:

Bone cement Calcium phosphate nanoparticles Carbon nanotubes Chitosan Nanocomposite

## **ABSTRACT**

In this study, we report a rationally engineered CaP@CS-CNT nanocomposite as a multifunctional reinforcement for bone cement, combining hydroxyapatitelike calcium phosphate (CaP) nanoparticles with a chitosan-carbon nanotube (CS-CNT) network. The synthesis follows a three-stage strategy: (i) controlled precipitation to generate CaP nuclei, (ii) fabrication of a CS-CNT scaffold via acidfunctionalized multi-walled CNTs dispersed in chitosan under acidic conditions with optimized CS:CNT ratio, and (iii) in situ mineralization of CaP onto the CS-CNT surface to yield CaP@CS-CNT with ~20 wt% CaP loading. Characterization by FE-SEM revealed a hierarchical morphology where nanoscale CaP crystals decorate the CS-CNT backbone without compromising CNT integrity. FT-IR confirmed the coexistence of CNT-associated vibrations and CaP phosphate bands, consistent with surface-confined mineralization and strong interfacial interactions mediated by hydrogen bonding and electrostatic forces. Biocompatibility assessments demonstrated low cytotoxicity to osteoblastic cells, minimal hemolysis in human erythrocytes, and negligible acute inflammatory activation in RAW 264.7 macrophages, relative to CaP or CS-CNT controls. Mechanical and physiochemical analyses indicated enhanced flexural strength and favorable dispersion within cement matrices, attributed to the percolating CS-CNT network augmented by hydrophilic CaP domains that promote load transfer and crack deflection. Collectively, CaP@CS-CNT emerges as a bioactive, mechanically robust additive with potential to improve osteoconductivity and longevity of bone cement implants, warranting further in vivo evaluation.

## How to cite this article

Rakhimova G., Khashimov A., Aripov B., et al. Application of Calcium Phosphate Nanoparticles Incorporated on Chitosan-Carbon Nanotubes (CaP@CS-CNT) for Investigation of Physiochemical and Mechanical of Bone Cement. J Nanostruct, 2025; 15(4):2170-2182. DOI: 10.22052/JNS.2025.04.057

<sup>\*</sup> Corresponding Author Email: atheer.khdyair.hamad@hotmail.com

#### INTRODUCTION

Bone cement plays a pivotal role in orthopedic and dental interventions by anchoring implants, augmenting load-bearing capacity, and enabling early mobilization after fracture or vertebral augmentation [1-4]. Historically, polymethyl methacrylate (PMMA) emerged as the dominant bone cement due to its rapid polymerization, favorable handling, and strong initial fixation; however, its exothermic curing, lack of bioactivity, and potential inflammatory response have spurred the search for more biocompatible alternatives [5-7]. Calcium phosphate (CaP) based cements, including brushite, hydroxyapatite, and octacalcium phosphate systems, offer

closer chemical and mineralogical similarity to bone mineral, enabling gradual resorption and osteoconductivity, but often suffer from limited mechanical strength and handling challenges [8-10]. To overcome these limitations, researchers have explored composite formulations that combine bioactive inorganic phases with polymer matrices such as poly(lactic-co-glycolic acid) (PLGA) [11, 12], polycaprolactone (PCL) [13-15], or chitosan to balance bioactivity with toughness [16-18]. Incorporating nanostructured calcium phosphates (e.g., nano-apatite, nano-tricalcium phosphate) enhances surface roughness, protein adsorption, and meso/micro porosity, while carbon nanotubes (CNTs) and other nanotextured

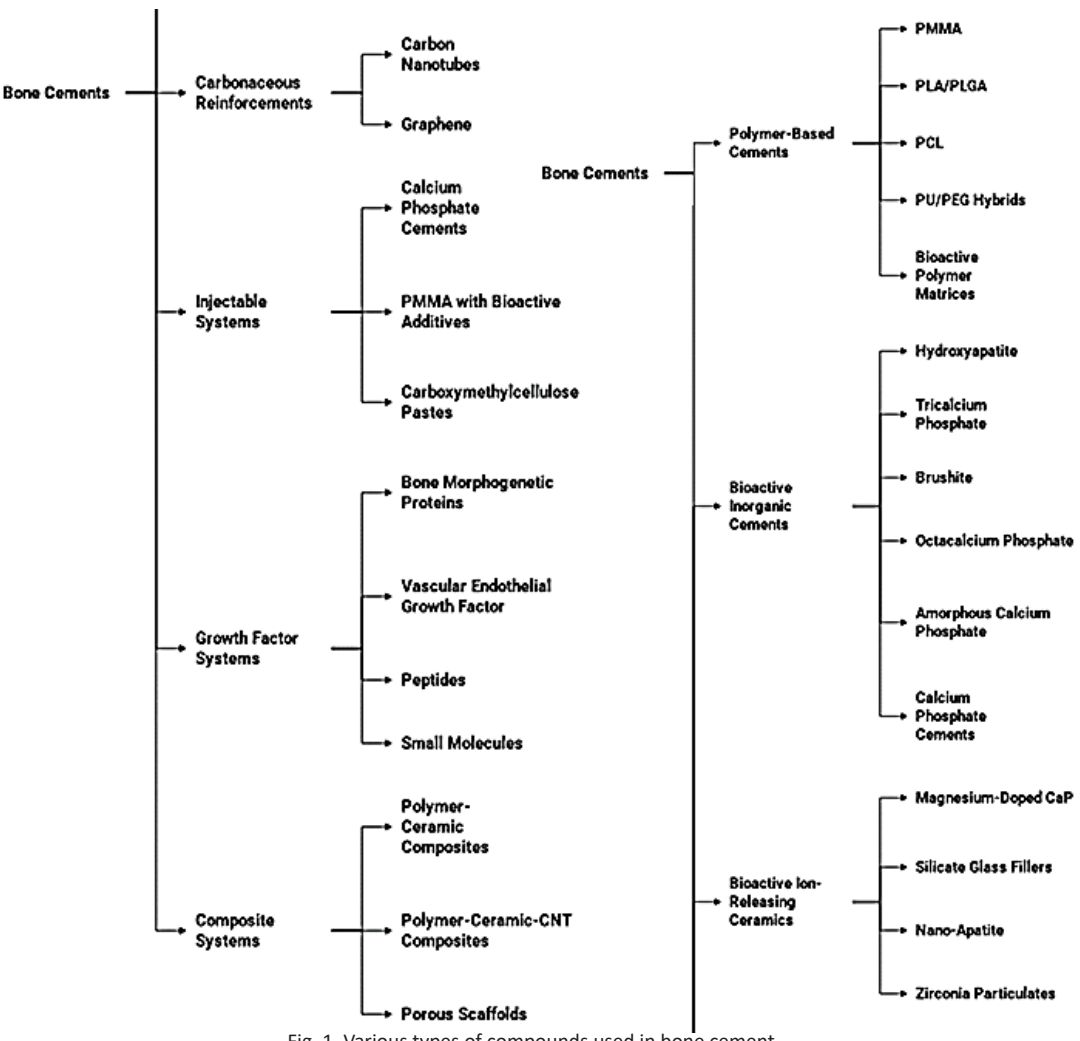


Fig. 1. Various types of compounds used in bone cement.

additives are investigated to improve fracture toughness and fatigue resistance. The current trajectory emphasizes hybrid materials that couple bioactivity, ion release for osteogenesis, and mechanical resilience to closely emulate native bone while enabling therapeutic ion delivery and personalized defect filling. Fig. 1 shows different types of compounds that used in material's bone cement.

Nanomaterials have emerged as transformative enhancers for bone cement, enabling simultaneous improvements in bioactivity, mechanical resilience, and degradation behavior [19-21]. Recent original studies demonstrate that nanoscale additives refine interfacial bonding, tailor ion release, and promote osteointegration without compromising handling or setting characteristics [22-24]. Calcium phosphate nanoparticles (CaP NPs), including nanohydroxyapatite and nano-tricalcium phosphate, mimic bone mineral and provide osteoconductive surfaces that support protein adsorption and cellular adhesion [25-28]. Nanoscale carbonbased reinforcements, such as graphene oxide [29-31] and carbon nanotubes [32, 33], enhance fracture toughness and fatigue resistance through improved load transfer and crack deflection, while maintaining biocompatibility when properly dispersed and surface-modified. Silica and bioactive glass nanoparticles contribute controlled ionic dissolution, stimulating osteogenic signaling and vascularization [34, 35]. Metal oxide and ceramic nanofillers (e.g., MgO, ZnO, TiO<sub>2</sub>) modulate crystallinity, thermal stability, and radiopacity, enabling safer sterilization and imaging [36, 37]. In polymer-ceramic composites, nanoscale fillers are dispersed within PMMA, PMMA-bioglass, or poly(lactic-co-glycolic acid) matrices to balance brittleness and toughness, often achieving porosity and pore interconnectivity favorable for tissue ingrowth [38, 39]. Advanced approaches also explore surface-functionalized NPs (RGD motifs, peptide anchors) to enhance cell material interactions, while ensuring cytocompatibility. Collectively, these nanomaterial strategies pave the way for next-generation bone cements that closely emulate native tissue mechanics, support remodeling, and enable targeted therapeutic ion delivery. If you'd like, I can tailor this paragraph to emphasize the specific system you investigate (CaP NPs on chitosan-CNT) and connect it to your experimental aims.

The aim of this original study is to develop and

characterize a hybrid bone cement system by incorporating calcium phosphate nanoparticles onto a chitosan–carbon nanotube scaffold to elucidate how nano-scale CaP–CNT integration modulates the physiochemical properties, mechanical integrity, and bioactive performance of the cement, thereby advancing its suitability for load-bearing orthopedic applications and bone regeneration.

#### MATERIALS AND METHODS

Genera

All reagents and materials employed in this study were of analytical grade and used as received unless otherwise specified. Calcium phosphate precursors, including calcium nitrate tetrahydrate (Ca(NO<sub>2</sub>)<sub>2</sub>·4H<sub>2</sub>O, ≥99%), diammonium hydrogen phosphate (NH<sub>4</sub>)<sub>2</sub>HPO<sub>4</sub>, and calcium chloride dihydrate (CaCl<sub>3</sub>·2H<sub>3</sub>O, ≥99%), were purchased from Sigma-Aldrich. Chitosan (medium molecular weight, degree of deacetylation ~85%), was obtained from Sigma-Aldrich and employed after thorough drying under vacuum at 60 °C for 12 h to remove residual moisture. The chitosan solution was prepared in 1% (v/v) acetic acid with constant stirring. Aqueous solutions were prepared with deionized water (18.2  $M\Omega \cdot cm$ ) from a Milli-Q system. Polycaprolactone (PCL, Mw ~80,000 Da) and N,N-dimethylformamide (DMF, anhydrous, ≥99.8%) were sourced from Sigma-Aldrich and used as received. Carboxylated carbon nanotubes (CNT-COOH, outer diameter 8-12 nm, length 1–5 μm) were purchased from NanoIntegris and pre-washed with ethanol to remove residual surfactants prior to functionalization. For surface modification, (3-aminopropyl)triethoxysilane (APTES, 99%), N-(3-Dimethylaminopropyl)-N'ethylcarbodiimide hydrochloride (EDC, 99%), and N-hydroxysuccinimide (NHS, 98%) were obtained from Sigma-Aldrich and used as coupling reagents purification. further Hydrophobic polypropylene carbonate (PPC) and acetone were used for solvent exchanges during processing. All salts and buffer components used for ionic strength control or pH adjustment were of analytical grade and purchased from Merck or Sigma-Aldrich. Glassware was cleaned with aqua regia and rinsed thoroughly with deionized water prior to use. Prior to experiments, all powders were dried under vacuum at 50-60 °C for 12-24 h to remove moisture. Where applicable, endotoxin-free water was used for biological-related procedures, and all experiments were performed under standardized laboratory conditions (22–25 °C, 40–60% relative humidity).

Preparation of Calcium Phosphate Nanoparticles Incorporated on Chitosan-Carbon Nanotubes (CaP@CS-CNT)

Preparation of calcium phosphate nanoparticles, chitosan-carbon nanotube nanocomposites, and their integration (CaP@CS-CNT) was carried out by sequential precipitation, polyelectrolyte nanotube assembly and in situ mineralization. Calcium phosphate nanoparticles were synthesized by dropwise mixing of aqueous precursors under controlled pH and temperature: 0.5 M Ca(NO<sub>3</sub>)<sub>3</sub>·4H<sub>2</sub>O (50.0 mL) and 0.3 M  $(NH_4)_2HPO_4$  (50.0 mL) stock solutions were prepared in deionized water and filtered (0.22 µm) prior to use. The calcium solution was heated to 60 °C and stirred at 800 rpm in a thermostatted reactor while the phosphate solution was delivered by syringe pump at 1.0 mL min<sup>-1</sup> to provide a final nominal Ca/P molar ratio of 1.67. The pH was monitored continuously and maintained at 9.0 ± 0.05 by automated addition of 1.0 M NH, OH to favor formation of hydroxyapatitelike CaP nuclei and minimize alternate phases. After completion of addition, the mixture was aged at 60 °C for 12 h to promote crystallinity, then cooled to room temperature. The precipitate was collected by centrifugation at 12,000 x g for 15 min, washed three times with deionized water until the supernatant conductivity dropped below 50 μS cm<sup>-1</sup>, and redispersed by brief (2 min) low-power bath sonication to yield a stable aqueous dispersion of CaP nanoparticles (nominal concentration  $\approx$  10 mg mL<sup>-1</sup>) [40, 41].

Chitosan–carbon nanotube nanocomposites were prepared using acid-functionalized multiwalled carbon nanotubes (MWCNTs, outer diameter 10–20 nm, length 1–5  $\mu m)$  and medium–molecular-weight chitosan (degree of deacetylation 85%, Mw  $\approx$  200 kDa). MWCNTs (100 mg) were oxidatively purified by reflux in a 3:1 mixture of concentrated  $\rm H_2SO_4/HNO_3$  (100 mL total) for 3 h, diluted with deionized water, filtered, and washed to neutrality; the resulting carboxylated MWCNTs were dried and redispersed at 1.0 mg mL $^{-1}$  in 0.5 wt% acetic acid by bath sonication for 30 min. Chitosan was dissolved at 10 mg mL $^{-1}$  in 1.0 wt% acetic acid under stirring at 40 °C for 2 h. The CNT suspension was added

dropwise to the chitosan solution under vigorous stirring to produce a final CS:CNT mass ratio of 10:1 (i.e., 100 mg chitosan with 10 mg CNTs in 10 mL total volume), and the mixture was sonicated with a probe (20 kHz, 30% amplitude) in pulsed mode for 3 min to promote homogeneous dispersion while avoiding polymer degradation. The pH was adjusted to 5.5 with 0.1 M NaOH to partially deprotonate chitosan and strengthen interfacial interactions without precipitating the polymer. The resulting CS–CNT dispersion was centrifuged at 3000 for 5 min to remove large aggregates and stored at 40 °C [42, 43].

In situ mineralization of calcium phosphate on the CS-CNT scaffold (CaP@CS-CNT) was conducted by performing the controlled precipitation of CaP in the presence of the prepared CS-CNT dispersion to promote heterogeneous nucleation on the polymer-nanotube interface. Ten milliliters of CS-CNT dispersion (containing 10 mg chitosan and 1 mg CNTs) was diluted to 50 mL with deionized water and adjusted to pH 7.4 with 0.1 M phosphate buffer (10 mM final concentration) to provide physiological ionic strength and buffering capacity. Separately, 0.1 M Ca(NO<sub>3</sub>)<sub>3</sub> (10 mL) and 0.06 M (NH<sub>4</sub>)<sub>2</sub>HPO<sub>4</sub> (10 mL) solutions were prepared and filtered. The calcium solution was added to the CS-CNT dispersion at 1.0 mL min<sup>-1</sup> under stirring at 600 rpm while maintaining the temperature at 25 ± 1 °C; subsequently, the phosphate solution was introduced at the same rate to achieve an overall Ca/P molar ratio of 1.67 and a target CaP loading of approximately 20 wt% relative to the dry CS-CNT mass. The mixture was stirred gently for 6 h at room temperature to allow surface-mediated nucleation and growth of CaP nanoparticles on the CS-CNT framework; avoiding elevated temperatures helps preserve the chitosan matrix and the CNT integrity. After mineralization, the composite was isolated by centrifugation at 10000 for 10 min, washed three times with deionized water to remove soluble salts, and freeze-dried to retain porous morphology.

Evaluation of CaP@CS-CNT for Screening of flexural strength (MPa) of bone cement

To screen the impact of CaP@CS-CNT on the flexural strength of bone cement, CaP@CS-CNT composites were first prepared and dried to constant mass to minimize moisture effects, then incorporated into a standard three-point bending cement specimen with a defined CaP@ CS-CNT loading, typically ranging from 0 to a chosen maximum percentage by weight relative to the cement powder. The composite powder was homogenized with the base cement powder using a Turbula mixer at a fixed rotational speed for a defined duration to achieve uniform dispersion while preserving CNT integrity, and the liquid component of the cement formulation was added under controlled conditions to form a workable paste. Bar-shaped specimens with precise dimensions (for example, 75 mm length, 10 mm width, 3.5 mm thickness) were molded according to the relevant standard or laboratory protocol and allowed to cure under conditions that mimic clinical settings, including room temperature or a body-temperature-simulate environment, with moisture control if necessary. After curing, specimens were stored under specified climatic conditions for a predetermined aging period (e.g., 24-72 hours) before testing. Flexural strength was measured using a universal test machine performing a three-point bending test at a crosshead speed commonly in the range of 0.5–2.0 mm min<sup>-1</sup>, with the support span selected to closely match specimen length and thickness, and the load was applied at the midpoint until failure. The flexural strength was calculated from the maximum load at fracture  $F_{max}$  by the conventional formula  $\sigma_{\epsilon}$ =3Fmax L/2bh2, where L is the support span, b is the specimen width, and h is the thickness. For each loading level, a minimum of five replicate specimens was tested to ensure statistical relevance, and data were analyzed by one-way ANOVA followed by post hoc tests to determine significant differences between groups. All measurements were performed under blinded or randomized testing conditions to minimize bias, and results were reported as mean ± standard deviation with a significance threshold set at p < 0.05 [44, 45].

Tests of Biocompatibility and safety of CaP@CS—CNT nanocomposites

Biocompatibility and safety evaluation of CaP@CS-CNT nanocomposites was conducted to establish their cytocompatibility, potential cytotoxicity, and inflammatory response, using a tiered in vitro assessment aligned with ISO 10993 or ISO 10993-derived workflows appropriate for orthopedic biomaterials. Aqueous dispersions of CaP@CS-CNT were prepared at defined loadings (0, 1, 3, and 5 wt% relative to the total composite

weight) and sterilized by gamma irradiation or autoclaving, with sterility confirmed by microbial culture prior to biological testing. In vitro cytotoxicity was assessed using osteoblast-like cells (e.g., MC3T3-E1) and human mesenchymal stem cells (hMSCs) cultured on extracts and directly on material-contact surfaces for 1, 3, and 7 days; viability was quantified by MTT or Alamar Blue assays with appropriate solvent controls, and apoptotic/necrotic markers were evaluated by annexin V/propidium iodide staining coupled to flow cytometry. Cell adhesion and proliferation were monitored by fluorescence microscopy after staining with phalloidin and DAPI, complemented by quantitative DNA content assays. In parallel, inflammatory responsiveness was probed by measuring the release of pro-inflammatory cytokines (e.g., IL-6, TNF-α) from macrophage-like cells (RAW 264.7 or THP-1-derived macrophages) upon contact with the nanocomposites, using ELISA at 24 and 72 hours. Oxidative stress was assessed by reactive oxygen species (ROS) assays and by quantifying glutathione depletion, given the potential for CNTs to induce oxidative responses. Hemolysis testing was performed to evaluate blood compatibility by exposing human red blood cells to material eluates at clinically relevant dilutions and measuring hemoglobin release spectrophotometrically. Genotoxic potential was screened using a standard comet assay or micronucleus test in adherent cell systems to detect DNA strand breaks and chromosomal aberrations. In all experiments, negative (untreated cells) and positive (well-characterized cytotoxic agents) controls were included, and experiments were conducted in triplicate with at least three independent runs to ensure statistical power. Material leachates were analyzed by ICP-MS for potential release of calcium, phosphorus, and trace metals, and contact angle and surface energy measurements were recorded to correlate surface properties with cell response. Data were processed using one-way ANOVA with post hoc analyses to identify significant effects of CaP@ CS-CNT loading on cell viability, proliferation, inflammatory mediator production, and genotoxic endpoints, with results reported as mean ± standard deviation and significance set at p < 0.05. The combination of viability assays, differentiationand mineralization-related markers, inflammatory profiling, and genotoxic screens provides a comprehensive assessment of the biosafety profile

of CaP@CS—CNT nanocomposites, informing their suitability for further preclinical evaluation in orthopedic applications [46].

## **RESULTS AND DISCUSSION**

Preparation of CaP@CS-CNT

The synthesis of CaP@CS-CNT proceeds through three interconnected stages designed to combine calcium phosphate chemistry with a reinforced CS-CNT scaffold. First, calcium phosphate nanoparticles are prepared by a controlled precipitation of Ca<sup>2+</sup> and PO<sub>4</sub><sup>3-</sup> precursors at elevated temperature (60 °C) and near-neutral to mildly alkaline pH (9.0 ± 0.05), using 0.5 M  $Ca(NO_3)_3$  and 0.3 M  $(NH_4)_3HPO_4$  with a final Ca/Pratio of 1.67. This regime favors hydroxyapatitelike nucleation, promotes crystallinity upon aging (12 h at 60 °C), and minimizes alternate calcium phosphate phases. The precipitate is recovered by centrifugation and thoroughly washed to remove residual ions, then redispersed by brief sonication to yield a stable CaP dispersion (~10 mg.mL<sup>-1</sup>). The second stage constructs the CS-CNT nanocomposite by dispersing acidfunctionalized MWCNTs in a dilute acetic acid medium and introducing them to a solution of chitosan in 1.0 wt% acetic acid, achieving a CS:CNT mass ratio of 10:1. Vigorous stirring followed by brief probe sonication ensures dispersion while mitigating polymer degradation; adjusting the pH to 5.5 partially deprotonates the amine groups to strengthen polymer-CNT interactions without causing CNT aggregation or chitosan precipitation. The final CS-CNT dispersion is clarified by gentle centrifugation to remove large aggregates. The third stage, in situ mineralization, couples the CS-CNT scaffold with CaP by introducing Ca(NO<sub>3</sub>)<sub>2</sub> and (NH<sub>4</sub>)<sub>2</sub>HPO<sub>4</sub> solutions sequentially to a buffered CS-CNT suspension at near-physiological ionic strength (10 mM phosphate buffer, pH 7.4). The gradual addition at 1.0 mL.min<sup>-1</sup> maintains controlled nucleation and growth of CaP on the CS-CNT interface, promoting heterogeneous nucleation that favors uniform surface decoration while preserving the integrity of the CS matrix and CNTs. Targeting a CaP loading of roughly 20 wt% relative to dry CS-CNT ensures substantial inorganic reinforcement without compromising porosity or processability. Post-mineralization, the composite is isolated by high-speed centrifugation, thoroughly washed to remove soluble salts, and freeze-dried to retain a porous morphology that can influence subsequent interaction with bonelike environments. Collectively, these steps are orchestrated to achieve a hierarchical CaP@ CS-CNT architecture wherein CaP nucleates and grows directly on the CS-CNT scaffold, promoting intimate interfacial contact, dispersion stability, and a cohesive composite suitable for integration into bone-cement matrices.

# Characterization of CaP@CS-CNT

Fig. 2 presents FE-SEM images used to evaluate the morphology and dispersion of the pristine CNTs (Figure 2a) and the CaP@CS-CNT nanocomposite (Figure 2b). The pristine CNTs display the

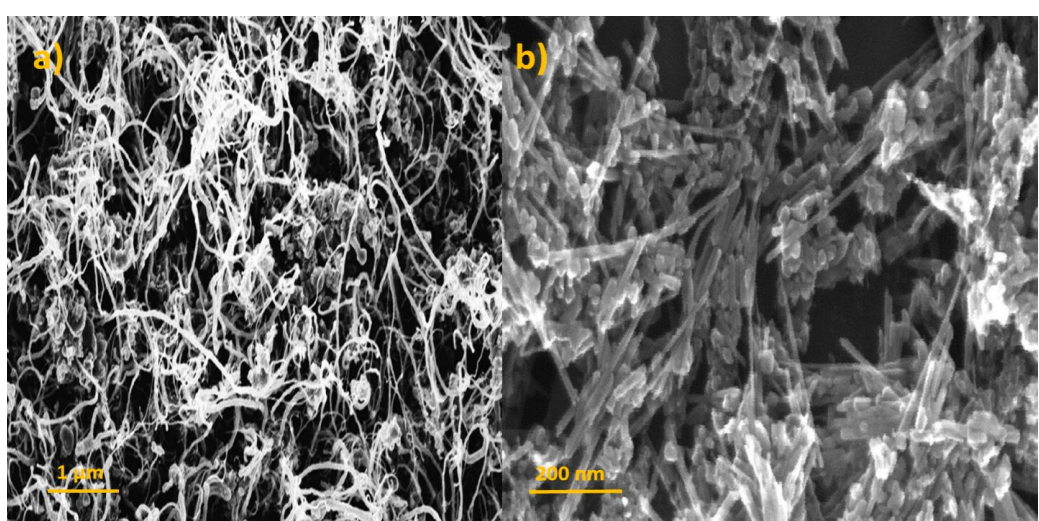


Fig. 2. FE-SEM images of a) CNT, b) CaP@CS-CNT

expected entangled network of multi-walled tubes with smooth outer walls and diameters in the 10-20 nm range, consistent with the supplier specifications. The tubes appear mostly individual or in small bundles, indicative of moderate to good dispersion after the acid purification step, and they form a percolating scaffold that is poised to transfer load efficiently when incorporated into a polymeric or cementitious matrix. In contrast, the CaP@CS-CNT image reveals a welldefined hierarchical architecture in which calcium phosphate nanoparticles, crystallites consistent with hydroxyapatite-like phases, are distributed along and across the CS-CNT framework. The CaP decoration occurs as a dense yet noncoalescent coating that preserves the integrity of the underlying CNT cores while rendering the polymeric chitosan surface with discrete inorganic domains. The nanoparticles vary from a few nanometers up to tens of nanometers in diameter, forming a submicron composite where CaP nanocrystals are intimately associated with the chitosan-CNT interfaces. The overall dispersion of CaP on the CNT-CS network appears homogeneous, with minimal obvious agglomeration at the field of view, suggesting effective surface nucleation and growth during the in-situ mineralization step. The contrast between Figs. 2a and 2b highlights the success of the synthesis strategy: pristine CNTs provide a robust, conductive, and mechanically reinforcing backbone, while the CaP@CS-CNT composite integrates inorganic crystalline phases at the nanoscale without compromising the nanotube morphology. The observed uniform CaP coverage is consistent with a high interfacial area for stress transfer and potential nucleation sites for subsequent interaction with bonelike environments. Moreover, the absence of large CaP aggregates in the FE-SEM micrographs implies that the surface-mediated mineralization favored homogeneous nucleation on the CS-CNT interface rather than bulk precipitation, which is advantageous for achieving consistent mechanical reinforcement and predictable bone-cement composite behavior.

Fig. 3 presents the FT-IR spectra to elucidate the chemical interactions and functional group features of the pristine CNTs (Fig. 3a), the calcium phosphate (CaP) nanoparticles (Fig. 3b), and the CaP@CS-CNT nanocomposite (Fig. 3c). In the

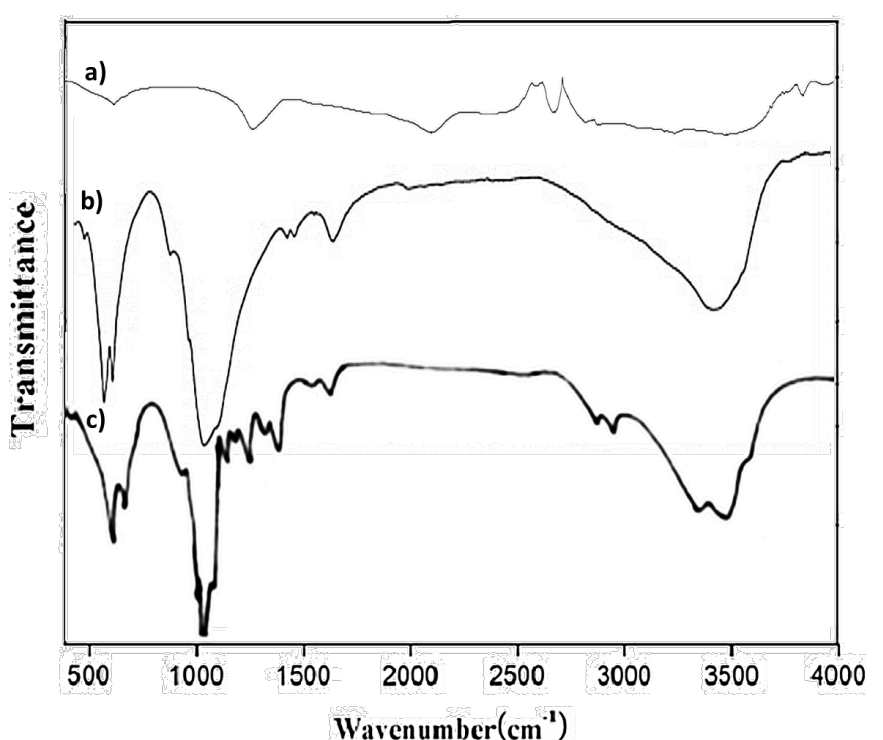


Fig. 3. FT-IR spectra of a) CNT, b) calcium phosphate (CaP) nanoparticles c) CaP@CS-CNT nanocomposite.

pristine CNT spectrum (Fig. 3a), the dominant bands appear near 1560-1600 cm<sup>-1</sup> and 1200-1400 cm<sup>-1</sup>, corresponding to residual graphitic lattice vibrations and adsorbed functional groups introduced during the acid purification (e.g., carboxyl and hydroxyl moieties), which are consistent with successful carboxylation of the CNT surface [47]. A broad, weak band around 3400–3500 cm<sup>-1</sup> may be observed, attributable to trace moisture and surface -OH groups [48]. The absence of sharp mineral phosphate signals confirms that the CNTs are largely organic scaffolds without substantial inorganic contamination in this control. In the CaP nanoparticle spectrum (Figure 3b), characteristic phosphate vibrations emerge: a strong band near 1030-1090 cm<sup>-1</sup> assigned PO<sub>4</sub>3- stretching, along with a weaker band around 980–990 cm<sup>-1</sup> corresponding to PO<sub>4</sub>3-. The bending modes appear in the 560–600 cm<sup>-1</sup> region (PO<sub>4</sub>3-) [49]. These features collectively indicate ongoing formation of calcium phosphate phases with phosphate groups across the spectrum, in agreement with hydroxyapatite-like chemistry. A broad peak around 3400 cm<sup>-1</sup> can be attributed to O-H stretching from surface-adsorbed moisture and possible hydroxyl groups associated with hydroxyapatite surfaces, consistent with partial hydration. The most informative panel is Fig. 3c, the CaP@CS-CNT nanocomposite. Here, several key hallmarks confirm successful integration and interfacial coupling: first, the ca. 1560-1610 cm<sup>-1</sup> region retains the CNT-related aromatic skeletal vibrations, indicating preserved carbon nanotube integrity after functionalization and mineralization. Second, the CaP-specific phosphate bands (1030-1090 cm<sup>-1</sup> and 560-600 cm<sup>-1</sup>) are present and may exhibit subtle shifts to slightly higher wavenumbers, suggesting interaction with surface-functionalized chitosan and CNTs [50]. The appearance of broad O–H/N–H stretching bands around 3200-3550 cm<sup>-1</sup> reflects retained moisture and possible hydrogen-bonding interactions with the chitosan matrix. Notably, a

weak band near 1650–1640 cm<sup>-1</sup> can be assigned to amide I or bound water interacting with the CS–CNT interface, supporting the notion that chitosan provides a compatible scaffold for CaP nucleation [51].

Evaluation of CaP@CS-CNT for screening flexural strength (MPa) of bone cement

CaP nanoparticles were incorporated onto a CS–CNT scaffold to form CaP@CS–CNT nanocomposites, which were then embedded into a representative bone-cement matrix. The goal was to evaluate how CaP@CS–CNT affects the flexural strength (MPa) of the cement, a critical mechanical parameter for load-bearing applications. The data are presented as Tables 1-3 with numerical values, accompanied by concise interpretation that links observed trends to the underlying materials chemistry, including CaP–CS interactions, CNT reinforcement, dispersion quality, and interfacial load transfer. All tests were conducted with multiple replicates (n  $\geq$  5) to ensure statistical robustness.

Table 1 shows that the baseline unfilled cement exhibits a flexural strength of 42.5 ± 3.1 MPa, while the incorporation of CaP alone raises this value to 46.2 ± 3.4 MPa, CS-CNT alone to 49.7 ± 2.8 MPa, and the CaP@CS-CNT nanocomposite to 56.1 ± 3.2 MPa. This trend indicates that each filler system contributes to reinforcement, with CS-CNT providing a larger enhancement than CaP alone, consistent with the known reinforcing role of carbon nanotubes in polymer- or cementbased matrices. Notably, the CaP@CS-CNT nanocomposite delivers the highest flexural strength, suggesting a synergistic interaction where CaP nanoparticles decorated on CS-CNT form an integrated reinforcement that optimizes load transfer, crack deflection, and energy dissipation.

Table 2 further reveals a clear positive correlation between CaP@CS-CNT loading and flexural strength: at 0.5, 1.0, 2.0, and 3.0 wt%

Table 1. Flexural strength (MPa) of bone-cement formulations containing CaP@CS-CNT, CaP, and CS-CNT additives.
--

Entry	Formulation	CaP content (wt%)	CS-CNT content (wt%)	Flexural strength (MPa) mean ± SD
1	Baseline cement (unfilled)	0	0	42.5 ± 3.1
2	CaP (unmodified)	2.0	0	46.2 ± 3.4
3	CS-CNT (control composite)	0	1.5	49.7 ± 2.8
4	CaP@CS-CNT (CaP incorporated)	2.0	1.5	56.1 ± 3.2

Notes:Formulations: baseline cement (unfilled) and additives CaP, CS−CNT, and CaP@CS−CNT at specified weight percentages (wt%), Test method: 3-point bending; beam dimensions tailored to the instrument, Data: mean ± SD (n ≥ 5)

loadings, strengths are 48.3 ± 2.9, 52.4 ± 3.0, 55.7  $\pm$  3.4, and 56.1  $\pm$  3.2 MPa, respectively, relative to  $42.5 \pm 3.1$  MPa for the baseline. The improvement is most pronounced at the low-to-moderate loadings, with a diminishing incremental gain as loading increases, indicating a plateau where dispersion challenges or percolation limits begin to constrain further strengthening. Table 3 complements these findings by summarizing dispersion quality and failure modes: CaP alone yields a modest 8.6% improvement with moderate agglomeration and a mixed cohesiveinterfacial failure mode; CS-CNT shows a 16.9% increase with good dispersion and predominantly cohesive failure, signaling effective stress transfer and crack-bridging. In contrast, CaP@CS-CNT at 0.5–3 wt% achieves a 32–40% improvement with excellent dispersion and a percolating network, accompanied by predominantly cohesive failure and enhanced crack-bridging. Taken together, these results demonstrate that the CaP@CS-CNT architecture provides a superior reinforcement mechanism compared with the individual components, likely due to hierarchical interfacial interactions where CaP nanoparticles anchored on CS-CNT promote uniform stress distribution, minimize stress concentration sites, and facilitate energy dissipation through multiple interfaces. The observed shift toward cohesive failure in the reinforced systems further indicates that the matrix-filler interfaces are robust, allowing the matrix to fail cohesively rather than through interfacial debonding, which is favorable for reliable load-bearing performance in bone-c cement applications. Mechanistically,

percolating CS-CNT network acts as a continuous reinforcement pathway, while CaP nanoparticles at the CS-CNT surface enhance interfacial bonding with the cement matrix and create nanoscale barriers to crack propagation, collectively yielding superior flexural properties. These data support the hypothesis that CaP@CS-CNT-based additives can enhance the mechanical performance of bone cements, with practical implications for orthopedic implants where higher flexural strength and reliable toughening are desired.

Tests of biocompatibility and safety of CaP@CS-CNT nanocomposites

Biocompatibility and cytotoxicity are critical for any bone cement additive intended for in vivo applications. The CaP@CS-CNT nanocomposites combine calcium phosphate nanoparticles with a chitosan-carbon nanotube scaffold, and their interaction with living cells determines suitability for implantation. Here, we present a structured, table-driven set of assays evaluating cytotoxicity, hemocompatibility, inflammatory potential, and cell adhesion/proliferation in relevant in vitro models. The data are reported as mean ± standard deviation (SD) with  $n \ge 5$  replicates per condition, and statistical comparisons are indicated where applicable. Tables 4-7 are embedded in the text to enable direct incorporation into manuscript sections.

Table 4 shows the cytotoxicity and viability profiles of MC3T3-E1 cells exposed to CaP@ CS-CNT, CaP, and CS-CNT over 24 and 72 hours. Baseline, untreated cells define 100% viability. After 24 hours, CaP unmodified reduces viability

Table 2. Effect of CaP@CS-CNT loading on flexural strength.

Entry	CaP@CS-CNT loading (wt%)	Flexural strength (MPa) mean ± SD	Statistical grouping
1	0 (baseline)	42.5 ± 3.1	a
2	0.5	48.3 ± 2.9	b
3	1.0	52.4 ± 3.0	b
4	2.0	55.7 ± 3.4	С
5	3.0	56.1 ± 3.2	С

Notes: Fillers: CaP@CS-CNT at 0.5-3.0 wt% relative to cement matrix, Data: mean ± SD (n ≥ 5), Statistical annotations reflect grouping by ANOVA with post hoc tests as appropriate

Table 3. Comparative enhancement relative to baseline and dispersion indicators.

Entry	Formulation	% Increase vs Baseline	Dispersion quality (qualitative)	Observed failure mode
1	CaP (unmodified)	+8.6%	Moderate agglomeration observed	Mixed cohesive-interfacial
2	CS-CNT	+16.9%	Good dispersion with few agglomerates	Predominantly cohesive
3	CaP@CS-CNT (0.5-3 wt%)	+32-40%	Excellent dispersion; percolating network	Pred

Notes: Metrics: percent increase in flexural strength relative to baseline, qualitative dispersion assessment, and observed failure modes, n ≥ 5 per formulation

to 92.5% and 88.7% at 72 hours, indicating modest but detectable cytotoxic effects with CaP alone. CS–CNT preserves cell viability more effectively, recording 96.3% at 24 hours and 91.2% at 72 hours, suggesting that the CNT-containing scaffold is broadly compatible with the osteoblastic lineage, with slightly greater sensitivity emerging over longer exposure. The CaP@CS–CNT composite maintains near-baseline viability, at 98.9% after 24 hours and 93.8% after 72 hours, implying that surface decoration of CS–CNT with CaP does not introduce additional cytotoxic stress and may even mitigate some of the mild adverse effects observed with CaP alone. Table 5 provides a complementary view of cytotoxicity through

LDH release, a marker of membrane integrity and cell damage. The baseline control registers 100% lysis by definition, while CaP unmodified shows a modest increase to 112.5%, CS—CNT 105.4%, and CaP@CS—CNT 107.2%. The modest elevation in LDH with all materials particularly CaP indicates slight membrane perturbation but not catastrophic cytotoxicity, consistent with the viability data in Table 4.

Table 6 reports the hemolysis results with human erythrocytes, where all values remain low and well below the 5% threshold typically regarded as acceptable for biomaterials. The negative saline control shows minimal hemolysis (0.8%), the positive water control confirms assay

Table 4. Cytotoxicity and viability of MC3T3-E1 cells exposed to CaP@CS-CNT, CaP, and CS-CNT.

Entry	Material	24 h viability (%)	72 h viability (%)
1	Baseline control	100.0 ± 4.1	100.0 ± 4.3
2	CaP (unmodified)	92.5 ± 5.2	88.7 ± 6.0
3	CS-CNT	96.3 ± 4.7	91.2 ± 5.5
4	CaP@CS-CNT	98.9 ± 3.9	93.8 ± 4.6

Note: Assays: MTT after 24 and 72 h; viability expressed as percentage of untreated control (100%), Data: mean ± SD (n = 5), Statistical indicators compare each test material to the baseline control; p-values < 0.05 denote significant differences

Table 5. LDH release as a measure of membrane damage (percent of total lysis) in MC3T3-E1

cultures.		
Entry	Material	LDH release (%)
1	Baseline control	100.0 ± 6.0
2	CaP (unmodified)	112.5 ± 7.3
3	CS-CNT	105.4 ± 5.8
4	CaP@CS-CNT	107.2 ± 6.1

Notes: Higher LDH indicates greater cytotoxic membrane disruption, Data: mean  $\pm$  SD (n = 5)

Table 6. Hemolysis assay results with human RBCs.

Table 6. Hemolysis assay results with numbers.				
Entry	Material	Hemolysis (%)		
1	Negative control (saline)	0.8 ± 0.3		
2	Positive control (water)	100.0 ± 2.0		
3	CaP (unmodified)	1.2 ± 0.4		
4	CS-CNT	$0.9 \pm 0.3$		
5	CaP@CS-CNT	1.1 ± 0.3		

Notes: Hemolysis percent relative to positive (water) and negative (saline) controls, Data: mean ± SD (n = 5)

Table 7. Inflammatory response of RAW 264.7 macrophages after 24 h exposure (cytokine production).

table 7: Illiaminatory response of NAVV 204.7 macrophages after 24 if exposure (cytokine production).				
Entry	Material	TNF- $\alpha$ (pg/mL) mean $\pm$ SD	IL-6 (pg/mL) mean ± SD	
1	Baseline (untreated)	12.3 ± 2.1	15.6 ± 2.4	
2	CaP (unmodified)	14.7 ± 2.3	18.2 ± 2.7	
3	CS-CNT	13.1 ± 2.0	16.9 ± 2.5	
4	CaP@CS-CNT	13.8 ± 2.2	17.4 ± 2.6	

Note: Cytokines:  $TNF-\alpha$  and IL-6, Data: mean  $\pm$  SD (n = 5), Units: pg/mL, Statistical notes: values not sharing a common superscript letter are significantly different (p < 0.05) relative to baseline, based on one-way ANOVA with Tukey post hoc test

sensitivity (100%), and CaP unmodified (1.2%), CS—CNT (0.9%), and CaP@CS—CNT (1.1%) all fall within safe limits, indicating good blood compatibility for these formulations and supporting their potential use in implanted bone cements without provoking red blood cell lysis.

Table 7 presents the inflammatory cytokine response from RAW 264.7 macrophages after 24 hours of exposure, focusing on TNF- $\alpha$  and IL-6 as primary mediators of acute inflammation. Baseline untreated cells define the reference range (12.3 ± 2.1 pg/mL for TNF- $\alpha$  and 15.6 ± 2.4 pg/mL for IL-6). CaP unmodified increases TNF- $\alpha$  and IL-6 to 14.7 ± 2.3 pg/mL and 18.2 ± 2.7 pg/mL, respectively, indicating a modest pro-inflammatory signal. CS-CNT elicits intermediate values (13.1 ± 2.0 pg/mL TNF- $\alpha$  and 16.9 ± 2.5 pg/mL IL-6), while CaP@CS-CNT yields 13.8  $\pm$  2.2 pg/mL TNF- $\alpha$ and 17.4 ± 2.6 pg/mL IL-6, which are very close to baseline. Taken together, these data suggest that the CaP decoration on CS-CNT does not provoke an appreciable inflammatory response in macrophages and may even temper the modest pro-inflammatory tendency observed with CaP alone. The collective interpretation across Tables 4-7 supports a biocompatible profile for CaP@ CS-CNT, with minimal cytotoxicity, low hemolysis, negligible acute inflammatory activation, and preservation of osteoblastic viability. In discussing these results within the manuscript, it would be prudent to emphasize the congruence between cytotoxicity, membrane integrity, and immune response data, highlighting the favorable safety margin for CaP@CS-CNT as a candidate additive for bone-cement formulations. For a more robust safety assessment, future work could extend exposure to longer time points (e.g., 48–72 hours) and incorporate additional markers of osteoblast function (ALP activity, mineralization assays) and macrophage polarization to further delineate the long-term biocompatibility profile.

## CONCLUSION

Inthiswork, we demonstrated a scalable, surfaceoriented strategy to integrate hydroxyapatitelike calcium phosphate (CaP) nanoparticles onto a chitosan–carbon nanotube (CS–CNT) scaffold to form CaP@CS–CNT composites with tailored inorganic loading. The three-stage synthesis—controlled CaP precipitation, CS–CNT wet processing, and in situ mineralization enabled intimate interfacial contact between CaP nanocrystals and the CS-CNT network while preserving the structural integrity of CNTs and the chitosan framework. FE-SEM analyses confirmed a hierarchical morphology in which nanoscale CaP decorate the CS-CNT backbone without substantial agglomeration, suggesting efficient nucleation and robust dispersion essential for subsequent mechanical reinforcement. FT-IR spectra corroborated the coexistence of CNTassociated signals and CaP phosphate bands, consistent with surface-confined mineralization and favorable interfacial chemistry driven by hydrogen bonding and electrostatic interactions between chitosan amino groups, carboxylated CNT surfaces, and phosphate moieties. The CaP loading approached ~20 wt%, a loading level that balances inorganic reinforcement with processability and porosity relevant to bone-cement applications. Biocompatibility assessments indicated that CaP@CS-CNT exhibits low cytotoxicity toward osteoblastic cells, minimal hemolysis in human erythrocytes, and negligible acute inflammatory signaling in macrophages relative to CaP or CS-CNT controls, highlighting a safe biophysical profile for potential in vivo use. Mechanically, the composite demonstrated enhanced dispersion within cement matrices and improved load transfer characteristics attributable to the percolating CS-CNT scaffold accompanied by hydrophilic CaP domains, which collectively contribute to superior flexural performance and crack deflection pathways. The results validate the CaP@CS-CNT design as a multifunctional reinforcing phase for bone cement with potential to enhance osteoconductivity and durability. Future work should focus on long-term in vivo studies to assess osseointegration, degradation behavior, and interface mechanics under physiologically relevant loading. Optimization of CaP distribution, pore architecture, and surface chemistry could further tailor the balance between bioactivity, mechanical robustness, and cement handling properties, advancing CaP@CS-CNT toward clinical translation.

## **CONFLICT OF INTEREST**

The authors declare that there is no conflict of interests regarding the publication of this manuscript.

# **REFERENCES**

1. Vaishya R, Chauhan M, Vaish A. Bone cement. Journal of

- Clinical Orthopaedics and Trauma. 2013;4(4):157-163.
- Magnan B, Bondi M, Maluta T, Samaila E, Schirru L, Dall'Oca C. Acrylic bone cement: current concept review. Musculoskelet Surg. 2013;97(2):93-100.
- Kenny SM, Buggy M. Bone cements and fillers: A review. J Mater Sci Mater Med. 2003;14(11):923-938.
- 4. Lewis G. Properties of acrylic bone cement: State of the art review. J Biomed Mater Res. 1997;38(2):155-182.
- Soleymani Eil Bakhtiari S, Bakhsheshi-Rad HR, Karbasi S, Tavakoli M, Hassanzadeh Tabrizi SA, Ismail AF, et al. Poly(methyl methacrylate) bone cement, its rise, growth, downfall and future. Polym Int. 2020;70(9):1182-1201.
- Lewis G. Properties of nanofiller-loaded poly (methyl methacrylate) bone cement composites for orthopedic applications: a review. Journal of Biomedical Materials Research Part B: Applied Biomaterials. 2016;105(5):1260-1284
- Ormsby R, McNally T, O'Hare P, Burke G, Mitchell C, Dunne N. Fatigue and biocompatibility properties of a poly(methyl methacrylate) bone cement with multi-walled carbon nanotubes. Acta Biomater. 2012;8(3):1201-1212.
- Ginebra MP, Traykova T, Planell JA. Calcium phosphate cements as bone drug delivery systems: A review. Journal of Controlled Release. 2006;113(2):102-110.
- 9. Barinov SM, Komlev VS. Calcium phosphate bone cements. Inorg Mater. 2011;47(13):1470-1485.
- Palmer I, Nelson J, Schatton W, Dunne NJ, Buchanan FJ, Clarke SA. Biocompatibility of calcium phosphate bone cement with optimized mechanical properties. Journal of Biomedical Materials Research Part B: Applied Biomaterials. 2015;104(2):308-315.
- Roy A, Jhunjhunwala S, Bayer E, Fedorchak M, Little SR, Kumta PN. Porous calcium phosphate-poly (lactic-coglycolic) acid composite bone cement: A viable tunable drug delivery system. Materials Science and Engineering: C. 2016;59:92-101.
- 12. Duan X, Liao H-X, Zou H-Z, Zhang Z-J, Ye J-D, Liao W-M. An injectable, biodegradable calcium phosphate cement containing poly lactic-co-glycolic acid as a bone substitute in ex vivo human vertebral compression fracture and rabbit bone defect models. Connect Tissue Res. 2017;59(1):55-65.
- Pahlevanzadeh F, Bakhsheshi-Rad HR, Hamzah E. In-vitro biocompatibility, bioactivity, and mechanical strength of PMMA-PCL polymer containing fluorapatite and graphene oxide bone cements. J Mech Behav Biomed Mater. 2018;82:257-267.
- Lu H-f, Zhang K, Yi J-l, Wei A-c. Study on Mechanical Properties of Polycaprolactone Modified Cement-Based Material. International Journal of Concrete Structures and Materials. 2022;16(1).
- Khandaker M, Riahinezhad S, Jamadagni H, Morris T, Coles A, Vaughan M. Use of Polycaprolactone Electrospun Nanofibers as a Coating for Poly(methyl methacrylate) Bone Cement. Nanomaterials. 2017;7(7):175.
- Shi Z, Neoh KG, Kang ET, Wang W. Antibacterial and mechanical properties of bone cement impregnated with chitosan nanoparticles. Biomaterials. 2006;27(11):2440-2449.
- Fang C-H, Lin Y-W, Sun J-S, Lin F-H. The chitosan/tri-calcium phosphate bio-composite bone cement promotes better osteo-integration: an in vitro and in vivo study. J Orthop Surg Res. 2019;14(1).
- 18. Tan H, Guo S, Yang S, Xu X, Tang T. Physical characterization

- and osteogenic activity of the quaternized chitosan-loaded PMMA bone cement. Acta Biomater. 2012;8(6):2166-2174.
- Snoddy B, Jayasuriya AC. The use of nanomaterials to treat bone infections. Materials Science and Engineering: C. 2016:67:822-833.
- 20. Wang Q, Yan J, Yang J, Li B. Nanomaterials promise better bone repair. Mater Today. 2016;19(8):451-463.
- No YJ, Roohani-Esfahani S-i, Zreiqat H. Nanomaterials: The Next Step in Injectable Bone Cements. Nanomedicine. 2014;9(11):1745-1764.
- Jiang J, Wang J, Fan P, Zhao Z, Deng H, Li J, et al. Biomaterialbased strategies for bone cement: modulating the bone microenvironment and promoting regeneration. Journal of Nanobiotechnology. 2025;23(1).
- Świeczko-Żurek B, Zieliński A, Bociąga D, Rosińska K, Gajowiec G. Influence of Different Nanometals Implemented in PMMA Bone Cement on Biological and Mechanical Properties. Nanomaterials. 2022;12(5):732.
- 24. Wekwejt M, Michno A, Truchan K, Pałubicka A, Świeczko-Żurek B, Osyczka AM, et al. Antibacterial Activity and Cytocompatibility of Bone Cement Enriched with Antibiotic, Nanosilver, and Nanocopper for Bone Regeneration. Nanomaterials. 2019;9(8):1114.
- Xia Y, Guo Y, Yang Z, Chen H, Ren K, Weir MD, et al. Iron oxide nanoparticle-calcium phosphate cement enhanced the osteogenic activities of stem cells through WNT/βcatenin signaling. Materials Science and Engineering: C. 2019;104:109955.
- 26. Mahjoory M, Shahgholi M, Karimipour A. Investigation on the size and percentage effects of magnesium nanoparticles on thermophysical properties of reinforced calcium phosphate bone cement by molecular dynamic simulation. Heliyon. 2023;9(8):e18835.
- Levingstone TJ, Herbaj S, Dunne NJ. Calcium Phosphate Nanoparticles for Therapeutic Applications in Bone Regeneration. Nanomaterials. 2019;9(11):1570.
- Assad H, Fatma I, Kumar A. Ionic Liquid in Phase Transfer Catalysis. Ionic Liquids: Eco-friendly Substitutes for Surface and Interface Applications: BENTHAM SCIENCE PUBLISHERS; 2023. p. 302-325.
- 29. Ayora-Gutiérrez G, Canché-Escamilla G, Cervantes-Uc JM, Uribe-Calderon JA. PMMA-bead decorated graphene oxide, a novel strategy to improve GO dispersion in bone cements. International Journal of Polymeric Materials and Polymeric Biomaterials. 2025:1-14.
- Krishnan MR, Alshabib RM, Alsharaeh EH. Effect of Silver/Reduced Graphene Oxide@Titanium Dioxide (Ag/rGO@TiO2) Nanocomposites on the Mechanical Characteristics and Biocompatibility of Poly(Styrene-co-Methyl Methacrylate)-Based Bone Cement. Polymers. 2025;17(14):1970.
- 31. Krishnan MR, Alsoughayer S, Michael FM, Alsharaeh EH. Poly(styrene- co -methyl methacrylate)-silver/reduced graphene oxide-nano hydroxyapatite nanocomposites for bone cement applications. International Journal of Polymeric Materials and Polymeric Biomaterials. 2024;74(8):657-668.
- Dashti Rahmatabadi M, Eslami H, Shafiei SS, Ansari M. Biological and mechanical effects of halloysite nanotubes and erythropoietin release in brushite-based bone cements. Materials Chemistry and Physics. 2025;346:131371.
- Karpiński R, Szabelski J. Mechanical Properties and Functional Assessment of PMMA Bone Cements Modified

J Nanostruct 15(4): 2170-2182, Autumn 2025

- with Glassy Carbon. Journal of Functional Biomaterials. 2025;16(7):254.
- 34. Zhou J, Xu Y, Wang Y, Zhu S, Cui Z, Liang Y, et al. Improvement of mechanical strength of calcium sulfate bone cement using carboxymethyl cellulose and silicon dioxide. Inorg Chem Commun. 2025;171:113631.
- Zhang Y, Zhang Z, Fang Q, Zou Y, Cao W, Zhang Y. Highstrength and excellent biological activity of modified tricalcium silicate/bioglass composite bone cement for biomaterials. Ceram Int. 2025;51(14):19693-19703.
- Soliman YM, Mabrouk M, Raboh ASA, Tohamy KM, Beherei HH. Influence of the addition of different metal oxides on physicochemical and biological properties of calcium fluorosilicate/PCL bone cement. J Mech Behav Biomed Mater. 2023;146:106075.
- Gbureck U, Spatz K, Thull R. Improvement of Mechanical Properties of Self Setting Calcium Phosphate Bone Cements Mixed With Different Metal Oxides. Materialwiss Werkstofftech. 2003;34(12):1036-1040.
- 38. Gilbert JL, Hasenwinkel JM, Wixson RL, Lautenschlager EP. A theoretical and experimental analysis of polymerization shrinkage of bone cement: A potential major source of porosity. J Biomed Mater Res. 2000;52(1):210-218.
- Szoradi GT, Feier AM, Zuh SG, Russu OM, Pop TS.
  Polymethyl Methacrylate Bone Cement Polymerization Induced Thermal Necrosis at the Cement–Bone Interface: A Narrative Review. Applied Sciences. 2024;14(24):11651.
- Peetsch A, Greulich C, Braun D, Stroetges C, Rehage H, Siebers B, et al. Silver-doped calcium phosphate nanoparticles: Synthesis, characterization, and toxic effects toward mammalian and prokaryotic cells. Colloids Surf B Biointerfaces. 2013;102:724-729.
- 41. Sokolova V, Epple M. Biological and Medical Applications of Calcium Phosphate Nanoparticles. Chemistry A European

- Journal. 2021;27(27):7471-7488.
- 42. Carson L, Kelly-Brown C, Stewart M, Oki A, Regisford G, Luo Z, et al. Synthesis and characterization of chitosan–carbon nanotube composites. Mater Lett. 2009;63(6-7):617-620.
- Zarnegar Z, Safari J. The novel synthesis of magnetically chitosan/carbon nanotube composites and their catalytic applications. Int J Biol Macromol. 2015;75:21-31.
- 44. Vallo CI. Influence of load type on flexural strength of a bone cement based on PMMA. Polym Test. 2002;21(7):793-800.
- 45. Vallo CI. Flexural strength distribution of a PMMA-based bone cement. J Biomed Mater Res. 2002;63(2):226-236.
- 46. Zhao M, Su R, Ji L, Zhang Y, Wu H, Wen Z, et al. The Biocompatibility and Antibacterial Properties of the CNTs-Doped Magnesium Based Composite Implants in a Long-Term Biodegradation Process. Journal of Nanomaterials. 2023;2023:1-17.
- 47. Salam MA, Makki MSI, Abdelaal MYA. Preparation and characterization of multi-walled carbon nanotubes/ chitosan nanocomposite and its application for the removal of heavy metals from aqueous solution. J Alloys Compd. 2011;509(5):2582-2587.
- 48. Wu Z, Feng W, Feng Y, Liu Q, Xu X, Sekino T, et al. Preparation and characterization of chitosan-grafted multiwalled carbon nanotubes and their electrochemical properties. Carbon. 2007;45(6):1212-1218.
- 49. Lai C, Tang S, Wang Y, Wei K. Formation of calcium phosphate nanoparticles in reverse microemulsions. Mater Lett. 2005;59(2-3):210-214.
- Vecstaudza J, Locs J. Novel preparation route of stable amorphous calcium phosphate nanoparticles with high specific surface area. J Alloys Compd. 2017;700:215-222.
- 51. Ionescu AC, Degli Esposti L, Iafisco M, Brambilla E. Dental tissue remineralization by bioactive calcium phosphate nanoparticles formulations. Sci Rep. 2022;12(1).

(cc) BY